Surface & Coatings Technology xxx (2014) xxx–xxx

Contents lists available at ScienceDirect

Surface & Coatings Technology

journal homepage: www.elsevier.com/locate/surfcoat

Interface microstructure across cladding of super duplex stainless steel with austenitic stainless steel buffer layer

Morteza Shamanian [a], Abbas Eghlimi [a,*], Masoomeh Eskandarian [b], Jerzy A. Szpunar [c]

[a] Department of Materials Engineering, Isfahan University of Technology, Isfahan 84156-83111, Iran
[b] Department of Materials Engineering, Shiraz University, Shiraz 71348-51154, Iran
[c] Department of Mechanical Engineering, University of Saskatchewan, Saskatoon, SK S7N 5A9, Canada

ARTICLE INFO

Article history:
Received 4 August 2014
Accepted in revised form 14 October 2014
Available online xxxx

Keywords:
Super duplex stainless steel
Austenite buffer layer
Microstructure
Electron backscatter diffraction
Transition zone
Grain boundary character distribution

ABSTRACT

The evolution of microstructure and texture across the fusion boundaries of a cladding produced by gas tungsten arc welding process was examined by optical microscopy, X-ray diffraction, electron backscatter diffraction, and energy-dispersive X-ray spectroscopy. The cladding comprised of high strength low alloy steel substrate, austenitic stainless steel buffer layer, and super duplex stainless steel top coating. Results indicated that the heat affected zone of the substrate mainly consisted of coarse polygonal ferrite grains. The transition zone, which was separated from the buffer layer by Type II boundaries, was comprised of a narrow austenitic–martensitic band. The microstructure of the buffer layer was characterized by vermicular ferrite which was replaced by lathy morphology adjacent the top coating. The buffer layer grains had <001> ND, i.e. normal direction, orientation near their interface with the substrate. The top coating was separated from the buffer layer by a distinct epitaxially grown austenitic layer. In none the cladding layers, the texture of the austenite was as strong as that of the ferrite. While in the buffer layer, the austenite grains had close Nishiyama–Wasserman orientation relationship with respect to the parent ferrite, Kurdjumov–Sachs relationship was observed across the top coating. Both the ferrite and austenite phases had significant fraction of low angle grain boundaries across the cladding, but the mount of austenite grain boundaries with high angle grain boundaries with low Σ special character was higher. Moreover, the austenite showed higher levels of stored energy in both layers. The total fraction of low Σ boundaries was also higher in the top coating compared to the buffer layer.

1. Introduction

Super duplex stainless steels (SDSSs) have dual-phase microstructure consisting of body-centered cubic (BCC) ferrite phase and face-centered cubic (FCC) austenite phase. This structure gives them an excellent combination of good mechanical properties and high corrosion resistance [1]. Since these steels contain low nickel content, they have a great economical potential to replace more expensive nickel-base super alloys in most of the ambient temperature applications [2,3], especially when they are overlaid on low-alloy steel substrates. Although weld surfacing is increasingly used to improve the life expectancy and to reduce the cost of engineering components, the cladding of SDSSs is associated with some challenges, especially the necessity to precisely control both the dilution and thermal cycles. One of the major drawbacks of high dilution in SDSS cladding is the formation of martensite band and fully austenitic structure adjacent the fusion boundary [4,5]. To reduce the ill effects of high dilution of the low carbon substrate, the use of austenitic stainless steel (ASS) buffer layer proved to be a great solution. Accordingly, high chromium, low nickel and low manganese filler metals such as AWS ER209, ER218, ER219, ER240, ER307, ER309L, ER312, and ER316 are commonly employed in various industries for joining dissimilar metals or as buffer layer in cladding and lining of components in service temperatures below 315 °C [6,7]. However, as the carbon content of the substrate increases, ASSs buffer layers should be replaced by nickel-based buffers to effectively impede carbon migration [8].

Recently, many authors [9–11] have investigated the interface morphology of dissimilar diffusion welds. Referring to literature, it is clear that many important properties, such as grain size, grain morphology, grain boundary character distribution (GBCD), and texture are dependent on microstructural features across the interface. In addition, microstructure at such complex boundaries can significantly influence both the weldability and service behavior [12]. Thus, deep understanding of structure across these interfaces is required for proper assessment of cladding adherence, service life prediction, and failure analysis. We previously investigated the interface structure between high strength low alloy (HSLA) steel substrate and SDSS top coating couple [13]. In the present paper we discuss the microstructural evolutions across the fusion boundaries of a similar SDSS cladding produced by deposition

* Corresponding author. Tel./fax: +98 9354819161.
E-mail address: a.eghlimi@ma.iut.ac.ir (A. Eghlimi).
URL:E-mail addresses:E-mail address: https://aeghlimi.materials.iut.ac.ir. (A. Eghlimi).

http://dx.doi.org/10.1016/j.surfcoat.2014.10.034
0257-8972/

of an ASS buffer layer. The results of this study are useful for prediction of microstructural features across cladding and dissimilar welding in carbon steel/ASS/SDSS systems.

2. Experimental procedure

2.1. Material

In this study, an ASS buffer layer and a SDSS top coating were cladded sequentially on a flat thermomechanically hot rolled high strength low alloy (HSLA) steel substrate. The chemical composition of the top coating, buffer layer, and substrate can be reviewed in Table 1. Ignoring the dilution, based on the equivalent ratio of chromium/nickel (Cr_{eq}/Ni_{eq}) calculated from Welding Research Council (WRC) 1992 diagram, the solidification mode of the substrate, buffer layer, and top coating was austenitic, ferritic–austenitic, and ferritic, respectively.

2.2. Welding process

Gas tungsten arc welding (GTAW) using a cold wire and commercially pure argon shielding gas was utilized to produce the double-layer beads on-plate cladding. Before the cladding process, the substrate surface was ground and then, washed with acetone to remove oxide scales and contaminants. As demonstrated schematically in Fig. 1, the cladding direction was chosen parallel to the substrate rolling direction (RD). The cladding parameters were chosen based on previous studies [14,15] and are summarized in Table 2.

2.3. Metallographic examinations

For metallographic analyses across the cladding, numerous transverse samples were cut and prepared by standard metallographic techniques (see Fig. 1). Then, the samples were electro-polished at 20 V direct current (DC) with a solution that consisted of 25 g CrO_3, 133 mL acetic acid, and 7 mL distilled water. The solution used for electro-polishing, etched the buffer layer and top coating, but did not change the substrate surface. Thus, 2% nital–4% picral solution was used to etch the substrate. For metallographic examination on top cladding, the top surface was electro-etched in 40% NaOH at 3–5 V DC. Stainless steel cathode was used in both electro-polishing and electro-etching.

To characterize the structures and chemical composition along the fusion boundaries, optical microscopy and Hitachi SU6600 field-emission gun scanning electron microscope (FEG-SEM) equipped with energy dispersion spectroscopy (EDS) were utilized.

The microhardness measurements were also conducted according to ASTM E384 standard from the substrate to the top coating. The microhardness was measured by applying a load of 200 gf in 10 s using a Buehler Micromet 5101 Vickers digital microhardness tester.

2.4. Quantitative X-ray diffraction texture analysis

To determine the texture of the parent substrate, X-ray diffraction (XRD) analysis was carried out using Bruker 2D system with Cu Kα radiation ($\lambda = 1.54056$ Å) over an area of approximately 800 μm in diameter. In XRD analysis, the incomplete experimental pole figures (PFs), i.e. PFs of (111), (200), (220), and (311) planes, were used to calculate the complete orientation distribution function (ODF).

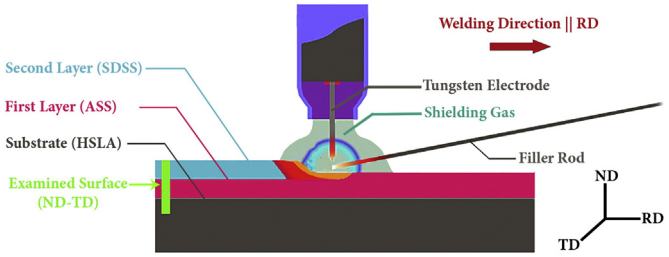

Fig. 1. Schematic representation of cladding process and examined surface area.

2.5. Electron backscatter diffraction analysis

In order to examine the GBCD, surface morphology and microstructure of the cladding, electron backscatter diffraction (EBSD) analysis was performed using Hitachi SU6600 FEG-SEM equipped with EBSD detector. To maximize the intensity of backscatter electrons and increase the number of possible diffraction events, samples were loaded in the SEM chamber at an angle of 70° from the incident beam toward the phosphor detector [16]. As illustrated in Fig. 1, the surface analyzed was laid on the ND–TD plane, where ND and TD are normal and transverse direction, respectively. In EBSD analysis, back-scattered electrons that form the diffraction patterns come from the top 10–50 nm of the surface. Thus, to avoid shadowing caused by topography, to minimize the plastic strain of the surfaces, and to ensure the smoothness of the surface, an accurate specimen preparation was performed. Accordingly, after grinding on diamond-bearing disks, the samples were polished with diamond-bearing paste and then chemically polished with a basic 50 nm colloidal silica slurry using VibroMet 2® vibratory polisher to remove the layers produced during mechanical polishing. After 6 h of lapping, the samples were rinsed in water, dried, and loaded in the SEM chamber.

For obtaining orientation maps, an accelerating voltage of 20 kV, working distance of 15 mm, and step size of 1 μm were used. To perform EBSD data visualization and post-processing, Kikuchi patterns were automatically analyzed using HKL CHANNEL5® software supplied by Oxford Instruments. The EBSD data was then used for various grain boundary and texture analysis across the three individual defined subsets, i.e. substrate, buffer layer, and top coating. To determine the preferential orientation relationship (OR), the PF of daughter phase, i.e. austenite, in the defined subsets was compared against the ideal PF of OR models which were calculated using GenOVa program [17,18].

Generally, deformed grains have higher dislocation densities and higher local misorientations within grains. Thus, kernel average neighbor misorientation (KANM) analysis was employed to evaluate the amount of residual strain. Since higher values were proven unnecessary, for a given pixel, the average misorientation of that point with respect to its 3rd nearest-neighbors was calculated in KANM analyses. In calculating the KANM, values above 5° threshold were excluded from the calculation, because these points were assumed to belong to adjacent grains [19].

3. Results and discussion

Since ferrite was a primary phase in solidification of buffer layer and top coating and this phase ensures a hot crack-resistance weld metal [1],

Table 1
Chemical composition of substrate, buffer layer and clad material (wt.%).

Material	C	Cr	Ni	Mo	N	Mn	Si	Cu	Ti	V	Nb	Cr_{eq}	Ni_{eq}	Cr_{eq}/Ni_{eq}
Substrate (API X65M)	0.26	0.02	–	0.05	–	1.36	0.41	0.05	0.02	0.01	0.01	**0.08**	**9.11**	**0.01**
Buffer layer (AWS ER309L)	0.01	23.5	14	–	–	1.8	0.4	–	–	–	–	**24.5**	**14.35**	**1.71**
Clad metal (AWS ER2594)	0.03	25.9	9.2	4.2	0.22	0.75	0.94	0.54	–	–	–	**30.1**	**14.64**	**2.06**

Please cite this article as: M. Shamanian, et al., Surf. Coat. Technol. (2014), http://dx.doi.org/10.1016/j.surfcoat.2014.10.034